GEOPHYSICAL RESEARCH LETTERS, VOL. 35, L03504, doi:10.1029/2007GL032692, 2008

Summer sea ice motion from the 18 GHz channel of AMSR-E and the exchange of sea ice between the Pacific and Atlantic sectors

Ron Kwok[1]

Received 15 November 2007; accepted 3 January 2008; published 5 February 2008.

[1] We demonstrate that sea ice motion in summer can be derived reliably from the 18GHz channel of the AMSR-E instrument on the EOS Aqua platform. The improved spatial resolution of this channel with its lower sensitivity to atmospheric moisture seems to have alleviated various issues that have plagued summer motion retrievals from shorter wavelength observations. Two spatial filters improve retrieval quality: one reduces some of the microwave signatures associated with synoptic-scale weather systems and the other removes outliers. Compared with daily buoy drifts, uncertainties in motion are ~3–4 km/day. Using the daily motion fields, we examine five years of summer ice area exchange between the Pacific and Atlantic sectors of the Arctic Ocean. With the sea-level pressure patterns during the summer of 2006 and 2007 favoring the export of sea ice into the Atlantic Sector, the regional outflow is ~21% and ~15% of the total sea ice retreat in the Pacific sector. **Citation:** Kwok, R. (2008), Summer sea ice motion from the 18 GHz channel of AMSR-E and the exchange of sea ice between the Pacific and Atlantic sectors, *Geophys. Res. Lett.*, *35*, L03504, doi:10.1029/2007GL032692.

1. Introduction

[2] For over a decade, daily fields of ice drift have been derived routinely from satellite passive microwave observations using tracking procedures devised by a number of investigators (listed in *Kwok et al.* [1998]). These motion fields, from the 85 GHz channel of the SSM/I (Special Sensor Microwave Imager) instrument, now span a period of >15 winters (October through May). This uninterrupted record of over a decade has been valuable for climate studies even though the uncertainties in the motion vectors are several kilometers per day. Launched in May 2002, the 89 GHz AMSR-E (Advanced Microwave Scanning Radiometer-EOS) radiometer on Aqua, with its twofold improvement over the lower resolution 85 GHz channel (~12 km) on the SSM/I instrument, adds to our ability to observe ice drift in smaller regions and in narrower channels and straits with reduced uncertainty.

[3] However, reliable estimates of sea ice motion from satellite passive microwave observations have been confined to the winter months because of the effects of weather, atmospheric moisture, and surface melt during the summer. These effects are particularly pronounced in the shorter wavelength passive microwave channels with the higher spatial resolutions necessary for accurate ice tracking. Currently, there are annual gaps of 3–4 months during the summer in our monitoring of the large-scale circulation pattern of the Arctic Ocean. The present note addresses summer ice motion retrieval from the 18 GHz channel of AMSR-E and the use of these fields to examine the role of ice advection in regional exchanges during the melt season. Specifically, we aim to: 1) demonstrate the retrieval of daily ice drift from the 18GHz and 36 GHz channels of the AMSR-E instrument during the summer; 2) quantify the uncertainty and coverage of the derived motion estimates and show that the 18 GHz retrievals are of better quality; and, 3) examine the advective area balance of the Arctic Ocean using the five years of summer ice motion (2003–2007) from this channel. The advective exchanges of sea ice between the Pacific and Atlantic sectors of the Arctic Ocean during the summer are compared to the large decline in summer ice coverage during the last five years.

2. Data Description

[4] The primary data sets include five summers (2003–2007) of: 1) gridded 12.5 km daily ice concentration estimates and brightness temperature (T_b) fields from AMSR-E radiometer on the NASA Aqua platform; 2) buoy drift from the International Arctic Buoy Program (IABP); and 3) daily sea level pressure (SLP) from the NCEP-NCAR analysis products. Of particular interest here are the T_b fields from the 18 GHz and 36 GHz channels with spatial resolutions of ~25 km and 12.5 km.

3. Ice Drift From AMSR-E

3.1. Ice-Tracking and "Weather" Filtering

[5] We follow the ice tracking procedure described by *Kwok et al.* [1998]. Briefly, the magnitude of the normalized cross-correlation coefficient is used as the measure of similarity between $n \times n$ pixel sub-images extracted from daily T_B fields. The 2D-spatial offset that maximizes the cross-correlation coefficient between the two time-separated sub-images gives the vector displacement. For the 18 GHz and 36 GHz T_b fields, the size of the square patches is ~133 km on a side. We sample the daily displacement vectors on a uniform grid of ~84 km resulting in an oversampled motion field. Motion estimates with the following attributes are considered low quality and discarded: 1) correlation peaks that are less than 0.3; and 2) motion vectors that are not within 60° of the local geostrophic wind direction. The tolerance of the directional filter is set rather high because of uncertainty in the quality of the wind fields and because ice motion is not entirely wind-driven.

[6] In the summer T_B fields, the relatively fast moving weather systems (relative to ice motion) over the Arctic Ocean typically appear as smooth long wavelength features

[1]Jet Propulsion Laboratory, California Institute of Technology, Pasadena, California, USA.

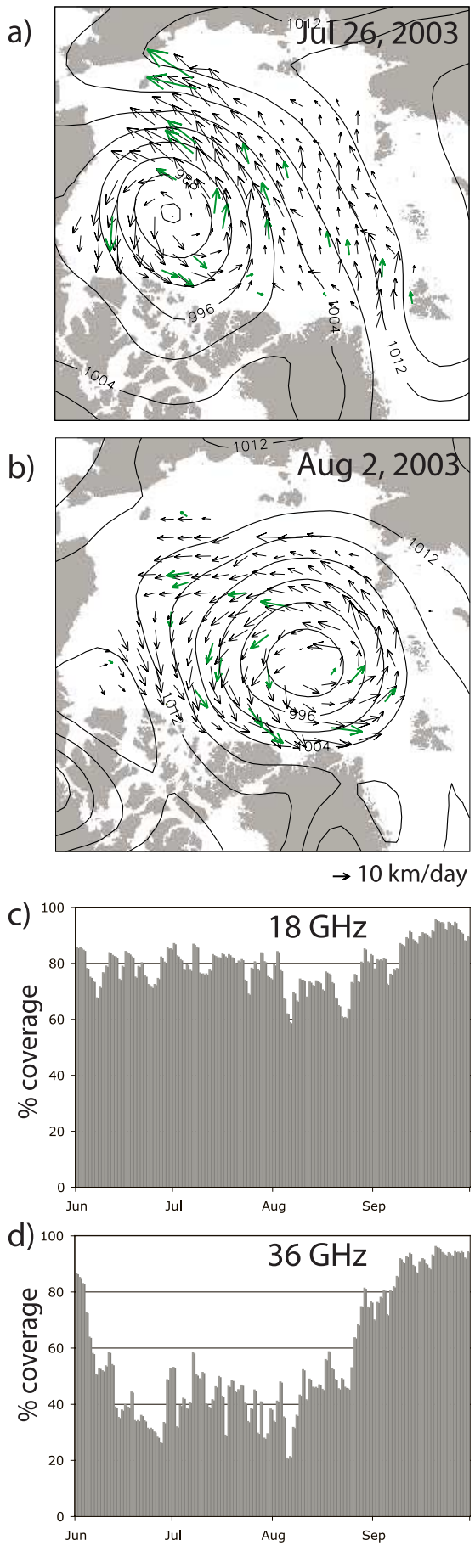

that modulate the more spatially variable ice surface signatures. Frequently, the ice tracker would lock on to the bands of moisture associated with atmospheric convergences or troughs. To reduce some of these effects, we introduce two 'weather' filters: one is applied to the T_B fields before the tracking step and the other to the motion field after the tracking step. In the pre-tracking filter, we subtract from the T_B fields a spatially smoothed version of itself - a 9 by 9 (or 112.5 km by 112.5 km) running mean of the T_B field. Equivalently, this is a high-pass filter that removes the variability of the T_B observations with wavelengths greater than ~112.5 km. This mitigates the effects of weather on the tracking process. The post-tracking filter discards motion vectors that are more than 5% of the geostrophic wind. Since ice motion is within 0–1% of the wind in the Arctic Ocean [*Thorndike and Colony*, 1982], displacements that are larger than 5% are most likely associated with tracking weather features. As seen in the assessment below, these filters seem to be effective in reducing the effects of weather in confounding the tracking process and in improving the quality of the overall motion estimates.

[7] Figures 1a and 1b show two sample fields of daily ice drift from the AMSR-E 18 GHz channel. The satellite motion fields plotted together with individual buoy drifts (in green) show the agreement between the two estimates. Quantitative assessment of these fields is provided in the next section. The SLP contours show that the circulation patterns are, as expected, approximately tangent to the isobars.

[8] The average daily coverage of the summer ice cover by the 18 and 36 GHz motion vectors (Figures 1c and 1d) from 5 years of daily estimates shows that even though it is possible to obtain motion estimates from the 36 GHz channel, the overall coverage of the ice extent is much better at 18 GHz. At the longer wavelength, the coverage is on average >70% of the ice cover; the lowest coverage of ~60% is in August. In contrast, we see a drastic decrease in the coverage by the 36 GHz estimates during the summer. The average coverage of this channel remains below 40% before recovering slowly at the end of August. Thus, the wavelength of choice for summer ice tracking is determined by the visibility of the ice surface in the AMSR-E T_B fields. The improved spatial resolution of the 18 GHz channel with its lower sensitivity to atmospheric moisture seems to have alleviated various issues that have plagued summer motion retrievals from the other microwave channels. There is very little difference in the results obtained from the V- and H-polarizations. Though not addressed here, there are residual effects on tracking due to time-varying surface melt that would tend to have an effect on the overall results.

3.2. Assessment of Ice Motion Estimates

[9] To assess the quality of the derived motion, we compare the daily drift estimates with buoy drifts. Since the sampling of the interpolated 12-hr buoy drifts coincides

Figure 1. Two examples of summer motion fields from the 18 GHz channel and the average daily coverage of the summer ice cover from 5 years of AMSR-E ice drift: (a) July 26, 2003 and (b) August 2, 2003. Buoy drift vectors are in green. Contours are sea level pressure isobars (interval: 2 hPa). (c) Area coverage (in percent) by 18 GHz motion estimates. (d) Coverage by 36 GHz motion estimates.

Table 1. Differences Between 18 GHz and 36 GHz AMSR-E Ice Motion and Daily Buoy Drift Before and After the Filters Described in the Text[a]

	$m_{\Delta x}$	$\sigma_{\Delta x}$	$m_{\Delta y}$	$\sigma_{\Delta y}$	$m_{\Delta\theta}$	$\sigma_{\Delta\theta}$	ρ^2	N
18 GHz								
Before filters								
Jun-Sep 03	0.0	4.2	0.8	5.0	3.9	28.2	0.74	1026
Jun-Sep 04	−0.1	5.4	−0.2	4.1	6.1	31.3	0.65	1180
Jun-Sep 05	−0.4	4.1	0.2	4.0	2.6	25.4	0.76	851
After filters								
Jun-Sep 03	0.3	3,3	0.3	3.4	6.7	17.5	0.86	1167
Jun-Sep 04	0.4	3.2	−0.1	3.4	9.0	18.3	0.85	820
Jun-Sep 05	−0.1	3.1	0.4	2.8	5.1	16.6	0.88	880
36 GHz								
Before filters								
Jun-Sep 03	−0.5	6.2	0.2	6.3	7.9	34.5	0.62	808
Jun-Sep 04	0.3	6.8	0.2	6.5	11.8	39.4	0.54	920
Jun-Sep 05	−1.0	5.6	0.1	5.0	6.2	31.9	0.65	886
After filters								
Jun-Sep 03	0.2	3.2	0.5	3.8	8.9	18.9	0.83	902
Jun-Sep 04	0.2	3.1	0.0	3.7	9.3	20.4	0.83	617
Jun-Sep 05	−0.3	3.2	0.3	3.0	5.8	17.7	0.86	741

[a]Units in km/day; $m_{\Delta x,\ \Delta y}$, $\sigma_{\Delta x,\ \Delta y}$, mean and standard deviation of the differences in the x and y directions; $m_{\Delta\theta}$, $\sigma_{\Delta\theta}$, mean and standard deviation of the directional differences; ρ^2, squared correlation between the two drift vectors; and N, number of samples.

approximately with the daily tracking results, no temporal interpolation is necessary. To align the two data sets spatially, the derived drift vectors are interpolated to the buoy locations. Differences between the daily 18 GHz, 36 GHz, and buoy drifts before and after the application of the 'weather' filters are summarized in Table 1. To reduce noise when the displacement estimates are small, differences are not computed when either the daily 18 GHz, 36 GHz, or buoy motion falls below 1 km/day. Three years of buoy drift in the Arctic Ocean from the IABP program are used here.

[10] Consistent improvements in the quality of the motion estimates before and after application of the filters, for all three years, are clear (see Table 1). While the differences have near zero means, the effectiveness of the filters can be seen in the decrease in the standard deviation of the daily displacement and directional differences and in the increase in squared correlation between buoy and satellite ice drift. At 18 GHz, while the velocity and directional uncertainties (in x and y) and squared correlations are between 4–5 km/day, ∼25°, and ∼0.7 before the filters, they are ∼3 km/day, <18°, and >0.85 after the filters. Similarly at 36 GHz, the velocity and directional uncertainties and squared correlations are ∼5.5 km/day, and ∼35°, and ∼0.6 before the filters, they are ∼3 km/day, <20° and ∼0.85 after the filters. The quality of the 36 GHz data is comparable to those of the 18 GHz after the application of the filters. But after accounting for coverage of the ice cover, as discussed above, the 18 GHz channel seems to provide better overall results.

4. Five Years of Summer Ice Motion

4.1. Patterns of Ice Drift

[11] The monthly mean ice motion fields from the five summers (June through September of 2003 to 2006) of AMSR-E 18 GHz observations are shown in Figure 2. Together with the monthly mean SLP isobars and the color-coded magnitude of ice drift (background), the variability of the summer ice motion over the five years can be clearly seen in the 18 GHz drift vectors.

[12] Broadly, there is a mix of cyclonic and anti-cyclonic circulation patterns in the 20 monthly fields of ice drift. Cyclonic patterns, with centers of low pressure inside the Arctic Ocean, are most pronounced in Jul-03, Aug-03, Sep-03, and Aug-06 fields. Anti-cyclonic patterns can be found in Jun-03, Jun-05, and the entire summer of 2007. Of the five years, the summer months of 2004 stand out as having the slowest ice motion (on average) and the lowest month-to-month variability. In both Sep-05 and Sep-06, the high density of isobars perpendicular to the Fram Strait is evident. These gradients in SLPs are associated with troughs of low pressure in the Barents and Norwegian Seas. Since ice motion is largely wind-driven and nearly parallel to the isobars of SLP, the result is an increase in sea ice outflow at the Fram Strait. The mean monthly ice motion for both Septembers are in excess of 7–8 km/day just north of the Strait. In Sep-05, the Transpolar drift stream associated with this arrangement of SLP favored the eastern Arctic Ocean as the source region of sea ice export, while the source region is shifted to the west in Sep-06. Recently, *Kwok* [2007] reports that the anomalously high Fram Strait ice export during the summer of 2005 explains ∼40% of the decrease in multiyear ice coverage of 0.6×10^6 km^2 between Jan-05 and Jan-06.

4.2. Ice Advection and Summer Retreat

[13] To examine the role of ice advection in the retreat of the ice cover during the summer of 2007, we contrast the ice area exchange between the Pacific and Atlantic Sectors (P-Sector; A-Sector) of the Arctic Ocean over the five summers. A line connecting the southwestern tip of Banks Island and the eastern most tip of Severnaya Zemlya divides the Arctic into the two sectors and serves as the gate where area exchanges are calculated. This gate spans a distance of ∼2840 km between the two endpoints. We consider the area of the Arctic Ocean covered by the two sectors as that bounded by the passageways into the Pacific, the Canadian Archipelago, and the Greenland and Barents Seas (see Figure 3a). Within these bounds of the Arctic Ocean, the area of the P- and A-Sectors are $\sim 4.2 \times 10^6$ km^2 and $\sim 3.0 \times 10^6$ km^2.

[14] During the summer, ice advection across the flux gate (defined above) alters the extent of melt within each sector. Increase/decrease in outflow from the P-Sector decreases/increases the actual area of melt in that sector. To obtain the actual area of summer melt in the P-Sector, the sea ice outflow has to be subtracted from the observed decrease in ice coverage. Figure 3 summarizes the role of inter-sector ice exchange on ice retreat in the P-Sector for the summers of 2003–2007. Line-plots (Figure 3) show the five years of summer ice coverage inside the two sectors (Pacific – blue; Atlantic – green) and the decrease in summer ice coverage of the P-Sector due to ice export (in red). Also shown are maps of the Arctic ice extent at the end of June (blue), July (green), August (red), and the September minimum (yellow) for the five summers. These maps show the rate of retreat of the ice cover during the four summer months.

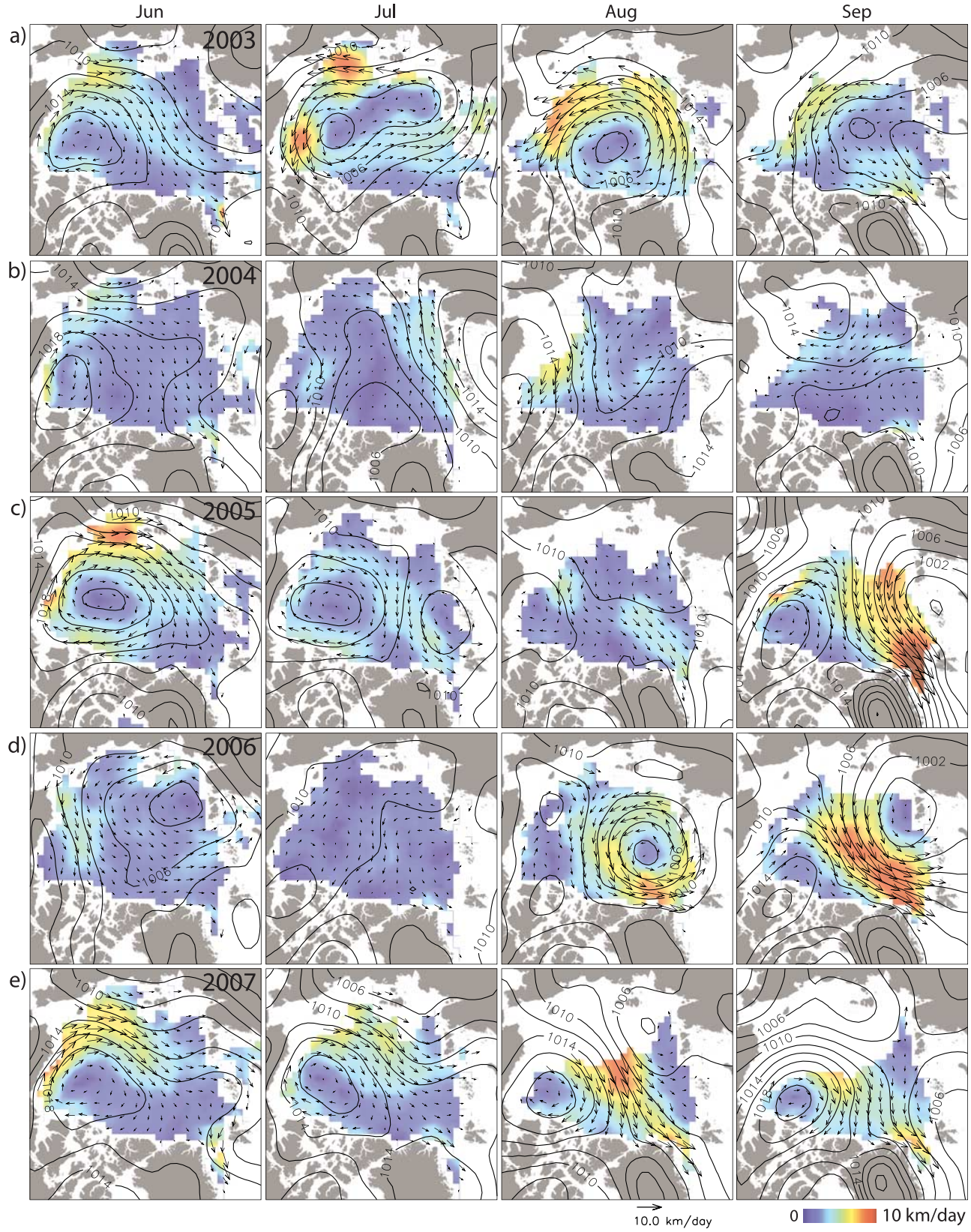

Figure 2. Five years of 18 GHz monthly mean motion fields for June, July, August, and September: (a) 2003, (b) 2004, (c) 2005, (d) 2006, and (e) 2007. Sea level pressure isobars are overlaid (contour intervals: 2 hPa).

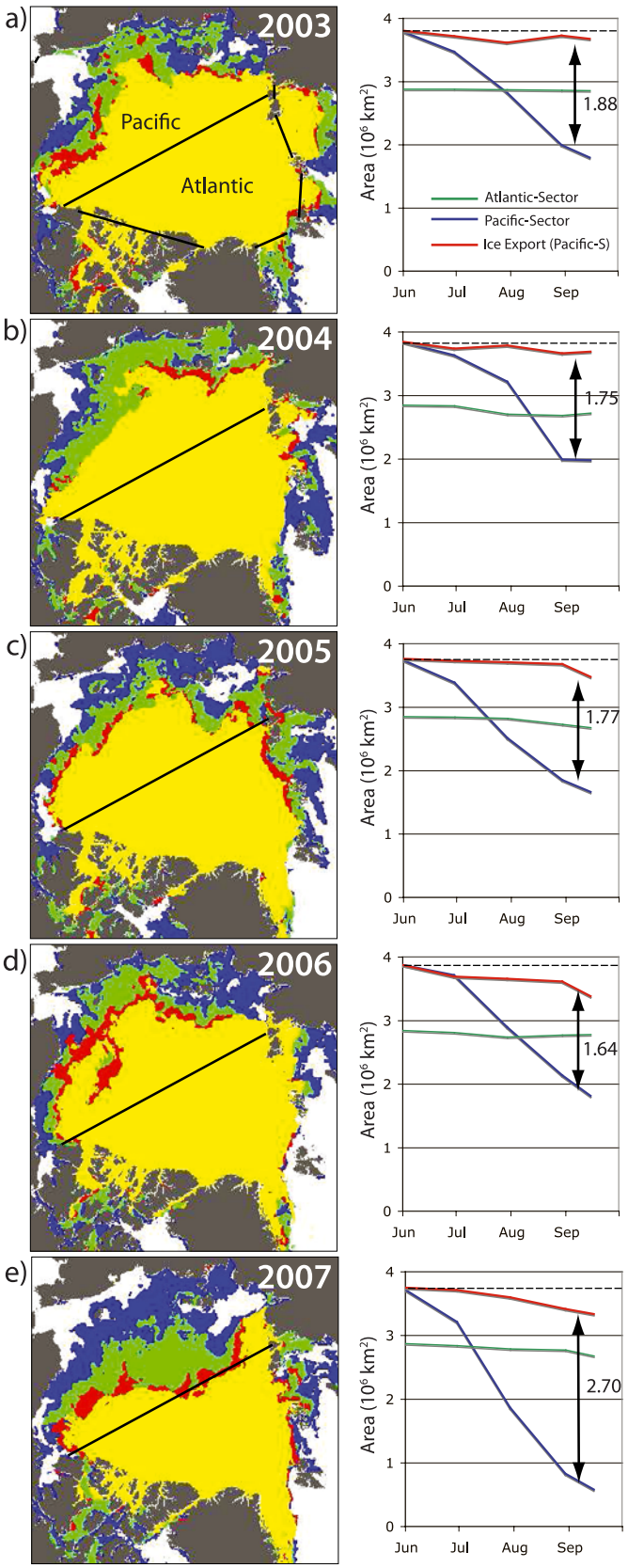

Figure 3. Maps of the Arctic ice extent at the end of June (blue), July (green), August (red), and the summer minimum (yellow) for the five summers. Line plots show the ice area in the two sectors (Pacific, blue; Atlantic, green) and the contribution of ice advection (in red) across the flux gate (defined above) to the summer retreat of sea ice in the Pacific: (a) 2003, (b) 2004, (c) 2005, (d) 2006 and (e) 2007. The flux gate, the bounds of the Arctic Ocean, and the two sectors (P-Pacific, A-Atlantic) are identified in Figure 3a.

[15] The net ice areas exported from the Pacific to the A-Sector for the five summers (2003–2007) are: 0.14, 0.12. 0.33, 0.43, and 0.48 $\times$ 10^6 km^2. This can be compared to the net decline in ice extent in the P-Sector of: 2.01, 1.87, 2.10, 2.07 and 3.17 $\times$ 10^6 km^2. The difference between these two quantities (shown in Figure 3) gives the actual melt area in the P-Sector. As a fraction (in percent) of the total area of summer retreat, the ice export accounts for 7%, 7%, 16%, 21%, and 15%. With summer ice motion from AMSR-E, we have been able to quantify the effect of ice advection on the observed summer retreat.

[16] Even though the P-Sector outflow in summer is only a fraction of the ice area retreat, the magnitude of the outflows during the three summers of 2005–07 is quite large relative to the average annual Fram Strait outflow of $\sim$0.87 $\times$ 10^6 km^2 [*Kwok et al.*, 2004], i.e., nearly 50%. In 2007, the value is greater than 50% of the average Fram outflow. As mentioned earlier, the increased outflows from the P-Sector and the Fram Strait during the summers of 2005 and 2006 are primarily associated with the SLP distribution during the month of September. In contrast, the summer of 2007 saw a persistent high-pressure pattern (Figure 2e) over the Canada Basin during the four summer months; this enhanced the advection of sea ice into the A-Sector. The consequence is that 2007 has the highest summer outflow into the A-Sector in this short record.

[17] What happens to this ice in the A-Sector? As seen in Figure 3 (line in green), the area of this sector within our Arctic Ocean bounds stays relatively stable over the five summers. Either ice export or ice convergence has to accommodate the inflow without significant changes in area. Area melt does not seem to be important because of the small negative trends. Using the relationship between monthly ice flux and sea-level pressure gradient across the Strait [*Kwok et al.*, 2004] to estimate the summer Fram Strait ice flux, we obtain the following Jun–Sep ice flux for 2005–2007: 0.25, 0.16, and 0.28 $\times$ 10^6 km^2. Even accounting for the small decline in summer ice coverage, these Fram exports are smaller than the ice inflow from the P-Sector; this suggests that outflows from the Atlantic Sector through the passageways into the Barents Sea and ice convergence must have to account for the balance. Indeed, the motion fields (Figure 2d) suggest that there are large outflows of sea ice into the Barents Sea in 2006 and that there seems to be significant convergence of sea ice onto the coast of northern Greenland and Ellesmere Island in 2007.

5. Conclusions

[18] In this note, we demonstrate that summer ice drift could be derived from the 18 GHz channel of the AMSR-E instrument. Assessed with daily buoy drifts, uncertainties in the estimates are $\sim$3–4 km/day. The 'weather' filters described herein show that they are relatively effective in conditioning the brightness temperature fields prior to the tracking process and the removal of outliers associated with weather after the tracking process. Compared to footprint of the 19GHz channel on SSM/I (resolution: 70 $\times$ 45 km), the improved spatial resolution of this channel (27 $\times$ 16 km) with its lower sensitivity to atmospheric moisture seems to have alleviated various issues that have plagued summer motion retrievals from the shorter wavelength microwave channels. This capability allows us to fill in the annual gaps of 3–4 summer months in our large-scale monitoring of Arctic Ocean sea ice circulation with satellite passive microwave observations and other AMSR-E channels [*Meier and Dai*, 2006; *Samelson et al.*, 2006].

[19] Using the ice drift from the past five summers, we examined the role of ice advection in the depletion of sea ice in the Pacific Sector of the Arctic Ocean, which in recent years has experienced significant summer melt. Increase/decrease in outflow from the Pacific Sector has to be accounted for in the calculation of the actual melt area. The net ice areas exported from the Pacific to the Atlantic-Sector for the five summers (2003–2007) are: 0.14, 0.12, 0.33, 0.43, and 0.48 $\times$ 10^6 km^2. The values are up to 50% of the annual Fram Strait ice outflow. As a fraction (in percent) of the total area of summer retreat, the ice export accounts for 7%, 7%, 16%, 21%, and 15%. In the overall Arctic Ocean area balance, these regional ice area exchanges have to be accounted for with either ice export, deformation or melt. The motion fields suggest large outflows of sea ice into the Barents Sea in 2006 and significant convergence of sea ice onto coasts of northern Greenland and Ellesmere Island in 2007.

[20] **Acknowledgments.** I wish to thank S. S. Pang for her assistance during the preparation of this manuscript. The AMSR-E brightness temperature and ice concentration fields were provided by World Data Center A for Glaciology/National Snow and Ice Data Center, University of Colorado, Boulder, CO. This work was performed at the Jet Propulsion Laboratory, California Institute of Technology under contract with the National Aeronautics and Space Administration.

References

Kwok, R. (2007), Near zero replenishment of the Arctic multiyear sea ice cover at the end of 2005 summer, *Geophys. Res. Lett.*, *34*, L05501, doi:10.1029/2006GL028737.

Kwok, R., A. Schweiger, D. A. Rothrock, S. Pang, and C. Kottmeier (1998), Sea ice motion from satellite passive microwave imagery assessed with ERS SAR and buoy motions, *J. Geophys. Res.*, *103*, 8191–8214.

Kwok, R., G. F. Cunningham, and S. S. Pang (2004), Fram Strait sea ice outflow, *J. Geophys. Res.*, *109*, C01009, doi:10.1029/2003JC001785.

Meier, W. N., and M. Dai (2006), High-resolution sea-ice motions from AMSR-E imagery, *Ann. Glaciol.*, *44*, 352–356.

Samelson, R. A., T. Agnew, H. Melling, and A. Münchow (2006), Evidence for atmospheric control of sea-ice motion through Nares Strait, *Geophys. Res. Lett.*, *33*, L02506, doi:10.1029/2005GL025016.

Thorndike, A. S., and R. Colony (1982), Sea ice motion in response to geostrophic winds, *J. Geophys. Res.*, *87*, 5845–5852.

R. Kwok, Jet Propulsion Laboratory, California Institute of Technology, Pasadena, CA 91109, USA. (ron.kwok@jpl.nasa.gov)